Redox Control of Exocytosis

Regulatory Role of NADPH, Thioredoxin, and Glutaredoxin

Rosita Ivarsson,[1] Roel Quintens,[2] Sandra Dejonghe,[3] Katsura Tsukamoto,[2] Peter in 't Veld,[3] Erik Renström,[1] and Frans C. Schuit[2]

Cellular redox state is an important metabolic variable, influencing many aspects of cell function like growth, apoptosis, and reductive biosynthesis. In this report, we identify NADPH as a candidate signaling molecule for exocytosis in neuroendocrine cells. In pancreatic β-cells, glucose acutely raised the NADPH-to-$NADP^+$ ratio and stimulated insulin release in parallel. Furthermore, intracellular addition of NADPH directly stimulated exocytosis of insulin granules. Effects of NADPH on exocytosis are proposed to be mediated by the redox proteins glutaredoxin (GRX) and thioredoxin (TRX) on the basis of the following evidence: *1*) Expression of GRX mRNA is very high in β-cells compared with other studied tissues, and GRX protein expression is high in islets and in brain; *2*) GRX and TRX are localized in distinct microdomains in the cytosol of β-cells; and *3*) microinjection of recombinant GRX potentiated effects of NADPH on exocytosis, whereas TRX antagonized the NADPH effect. We propose that the NADPH/GRX/TRX redox regulation mediates a novel signaling pathway of nutrient-induced insulin secretion. *Diabetes* 54: 2132–2142, 2005

Glucose-stimulated insulin release from pancreatic β-cells is a model for regulated exocytosis in neuroendocrine cells and one of great physiological importance (1–3). Glucose triggers exocytosis via closure of ATP-sensitive K^+ channels (K_{ATP} channels), causing a rise in cytosolic calcium (4). Pharmacological experiments indicated that K_{ATP} channel–independent pathways exist; however, the nature of which is unclear (5). When considering potentially relevant metabolic signaling molecules that may stimulate insulin release independently of closure of K_{ATP} channels, the redox state of β-cells has been correlated to secretory function (6,7), but the causal relation remains undetermined. In particular, the reduced pyridine nucleotides NADH and NADPH are interesting candidate regulators of exocytosis. First, upon stimulation with high glucose, a rapid shift of the redox state of individual pancreatic β-cells has been observed by fluorescence-activated cell sorting (7,8) as well as fluorescence microscopy techniques (9,10). The redox shift has been linked to a biochemically defined increase in cellular NADPH content (11–13). The difference in the redox state of individual β-cells (8) was associated to cellular heterogeneity in glucose metabolism (14). In addition to the acute effects, the chronic state of β-cell secretory performance has been correlated to the activity of metabolic pathways that are instrumental in either NADPH generation, such as citrate cataplerosis (15,16) and pyruvate cycling (17), or glycolysis coupled to mitochondrial NADH shuttle systems (18,19). To date, however, the cellular redox state and secretory capacity of the β-cell are correlated events without providing evidence if any of the redox nucleotides are directly responsible in the control of insulin release. To address these issues, we measured the acute effects of glucose on the cellular content of the individual nucleotides and assessed their efficacy in potentiating insulin exocytosis. Finally, as glutaredoxin (GRX) and thioredoxin (TRX) are the main redox acceptor proteins for NADPH electrons (20), we assessed the expression of these proteins in islet β-cells and investigated their functional role in NADPH-mediated exocytosis.

RESEARCH DESIGN AND METHODS

Cell purification and culture. Rat β-cells were purified from male Wistar rats after collagenase digestion of the pancreata, handpicking of the islets of Langerhans, dissociation of islets into single cells by trypsin in calcium-free medium, and autofluorescence-activated cell sorting (7,21). Cell purity and viability were ≥90%. β-Cells were reaggregated briefly and cultured for 16 h in serum-free Ham's F10 medium containing 1% BSA and 10 mmol/l glucose before experimentation. MIN6 cells (obtained from Drs. H. Ishihara and Y. Oka, Sendai, Japan), which are known to be glucose responsive in terms of metabolism and insulin release (22), were cultured in Dulbecco's modified Eagle's medium containing 25 mmol/l glucose and 15% heat-inactivated FCS. Cells were only used below passage number 33. INS-1E cells (passage 65) were cultured in RPMI 1640 medium supplemented with 10% FCS, 100 μg/ml penicillin, 100 μg/ml streptomycin, and 50 μmol/l 2-mercaptoethanol. PC12 cells were cultured in RPMI 1640 medium supplemented with 10 mmol/l HEPES, 1 mmol/l Na-pyruvate, 5% horse serum, 10% FCS, 100 IU/ml penicillin, and 0.1 mg/ml streptomycin. For RNA analysis, expression of GRX1 and TRX1 was studied in freshly isolated islet β-cells and non–β-cells and snap-frozen liver, muscle, fat, brain, pituitary, lung, and kidney from male Wistar rats. For Western blots, islets and control tissues were taken from female Sprague Dawley rats.

Measuring pyridine nucleotides. Pyridine nucleotides were extracted from batches of 1×10^5 rat β-cells and 2×10^5 MIN6 cells and quantified by

From the [1]Department of Physiological Sciences, Lund University, Lund, Sweden; the [2]Department of Molecular Cell Biology, Gene Expression Unit, Katholieke Universiteit Leuven, Leuven, Belgium; and the [3]Diabetes Research Center, Vrije Universiteit Brussels, Brussels, Belgium.

Address correspondence and reprint requests to Frans C. Schuit, Department of Molecular Cell Biology, Katholieke Universiteit Leuven, Herestraat 49, B-3000 Leuven, Belgium. E-mail: frans.schuit@med.kuleuven.ac.be or Erik Renström, Department of Physiological Sciences, Lund University, BMC B11, SE 22184 Lund, Sweden. E-mail: erik.renstrom@mphy.lu.se.

Received for publication 14 September 2004 and accepted in revised form 18 April 2005.

GRX, glutaredoxin; K_{ATP} channel, ATP-sensitive K^+ channel; TRX, thioredoxin.

TABLE 1
Oligonucleotide primers and probes used for real-time PCR analysis of GRX1 and TRX1 mRNA expression

Gene		Sequence (5′ to 3′)	Concentration
β-Actin	F	AGCCATGTACGTAGCCATCCA	900nmol/l
	R	TCTCCGGAGTCCATCACAATG	900nmol/l
	P	(FAM)TGTCCCTGTATGCCTCTGGTCGTAC(BHQ1)	50nmol/l
GRX1	F	CTGTCAGCATGGCTCAGGAGTTTG	300nmol/l
	R	CCACAAATTCCAGGAGACCACG	300nmol/l
	P	(FAM)TGGTCGTGTTCATCAAACCCACCTGC(TAMRA)	50nmol/l
TRX1	F	TCCAATGTGGTGTTCCTTGA	900nmol/l
	R	ATAGAACTGGAAGGTCGGCA	50nmol/l
	P	(JOE)AGCAACATCCTGGCAGTCATCCACG(TAMRA)	50nmol/l

FAM, 6-carboxyfluorescein; BHQ1, black hole quencher 1; TAMRA, 6-carboxytetramethylrhodamine; P, probe; F, forward; R, reverse.

enzymatic cycling (11). After a 30-min incubation in 0.5 ml of Earle's HEPES buffer (pH 7.35) containing 0.5% BSA and the indicated glucose concentration, cells were briefly centrifuged, and the supernatant fluid was aspirated. Pellets were frozen in liquid N_2 and homogenized by sonication for 1 min on ice in 50 μl 40 mmol/l NaOH/5 mmol/l cysteine solution. Sonicates were microfuged (30 s at 4°C), after which the supernatant fluid was distributed as follows: 10 μl + 5 μl 0.2M HCl (assay for $NADP^+$), 10 μl + 5 μl 40 mmol/l NaOH/5 mmol/l cysteine (NADPH), 10 μl + 5 μl 0.04M HCl (assay for NAD^+), and 15 μl undiluted extract (NADH analysis). After heating the samples for 10 min at 60°C, the enzymatic cycling reaction (1 h, 37°C) was started by adding 100 μl cycling reagent mixture per test sample. Enzymes were purchased from Boehringer Biochemicals, Mannheim, Germany. To lower the blank values of the NAD cycle, the malate and alcohol dehydrogenase stocks were treated by charcoal adsorption before use. The cycling reaction was stopped by heating for 3 min in a boiling water bath and 10 min centrifugation at 3,000 rpm. The indicator reaction was carried out fluorimetrically (excitation 340 nm/emission 460 nm) on a Hitachi F-2000 fluorimeter (Hitachi, Tokyo, Japan) using 90 μl of the cycling reaction product and adding 900 μl indicator reagent, measuring the amount of 6-phosphogluconolactone (NADP-cycle) or malate (NAD-cycle) formed during the cycling step. The appropriate pyridine nucleotide standard series were extracted in the same media as the unknown samples and run in parallel reaction tubes through the cycling and detection steps.

Insulin release. Insulin release was measured in the supernatant buffer of rat β-cells and MIN6 cells after 30-min static incubations in the same conditions as used for the pyridine nucleotide measurements. Cellular insulin content was measured after extraction of the cell pellet in 0.25% BSA in 2M acetic acid. Media and cellular insulin content was quantified via radioimmunoassay (21). Basal insulin release, determined at 1 mmol/l glucose concentration was subtracted from all release values to obtain glucose-induced release data.

Patch-clamp experiments. Isolated β-cells were prepared and whole-cell capacitance measurements were performed using EPC7/9 patch-clamp amplifiers with the software suite Pulse + X-Chart Extension (version 8.6 or later; HEKA, Lambrecht-Pfalz, Germany), as previously described (23,24). Primary islet cells or PC12 cells were seeded in Nunc plastic petri dishes and were used for experiments the following day. All chemicals were of analytical grade (Sigma). The extracellular solution contained 138 mmol/l NaCl, 5.6 mmol/l KCl, 2.6 mmol/l $CaCl_2$, 1.2 mmol/l $MgCl_2$, 5 mmol/l HEPES, and 5 mmol/l glucose (pH 7.4 with NaOH). In Figs. 3*A*–*F* and 7, 20 mmol/l tetra-ethyl-ammonium substituted for equimolar amounts of NaCl to block outward K^+ currents that otherwise obscured the (smaller) inward Ca^{2+} currents. The intracellular solution in Figs. 3*A*–*F* and 7 contained 125 mmol/l Cs-glutamate, 10 mmol/l CsCl, 10 mmol/l NaCl, 1 mmol/l $MgCl_2$, 5 mmol/l HEPES, 3 mmol/l Mg-ATP, 0.1 mmol/l cAMP, and 0.05 mmol/l EGTA, with NADPH added as indicated (pH 7.2 with CsOH). Cs^+ salts were used to block outward K^+ currents. In Fig. 3*G* and *H* and Fig. 4, the control intracellular solution consisted of 125 mmol/l K-glutamate, 10 mmol/l KCl, 10 mmol/l NaCl, 1 mmol/l $MgCl_2$, 5 mmol/l HEPES, 3 mmol/l Mg-ATP (except in Fig. 4*A* and *B*), 0.1 mmol/l cAMP, 10 mmol/l EGTA, and 9 mmol/l $CaCl_2$, with pyridine nucleotides added as indicated in text or figures (pH 7.2 with KOH). Recombinant rat GRX and TRX (IMCO, Stockholm, Sweden) were directly dissolved in the patch electrode solution to their final concentrations.

mRNA expression analysis. The mRNA expression profile of rat purified β-cells as well as from control tissues (liver, muscle, fat, brain, lung, pituitary, and kidney) were analyzed using rat 230A microarrays from Affymetrix (Santa Clara, CA). Total RNA was used to prepare biotinylated cRNA according to the standard Affymetrix protocol. Briefly, total RNA was reverse transcribed using the SuperScript Choice System (Invitrogen, Carlsbad, CA) via oligo-dT primers containing a T7 RNA polymerase promotor site. Complementary DNA was in vitro transcribed and labeled using the RNA transcript labeling kit (Enzo, Farmingdale, NY). The concentration of labeled cRNA was measured using the NanoDrop ND-1000 spectrophotometer. Labeled cRNA was fragmented in a fragmentation buffer during 35 min at 94°C. The quality of labeled and fragmented cRNA was analyzed using the Bioanalyzer 2100 (Agilent, Waldbronn, Germany). Fragmented cRNA was hybridized to the array during 16 h at 45°C. The arrays were washed and stained in a fluidics station (Affymetrix) and scanned using the Affymetrix 3000 GeneScanner. Raw data were analyzed using the Affymetrix GCOS software. Signal intensities were scaled using the global scaling method, taking 150 as target intensity value. Scaling factors were less than three times different from each other in all used arrays. Signal intensities for GRX and TRX were compared between individual arrays from β-cells ($n = 3$) on the one hand and the eight control tissues (islet non–β-cells, liver, muscle, fat, brain, pituitary, lung, and kidney; $n = 3$ each), allowing GCOS analysis of 72 pairwise comparisons between β-cell samples and the tissue samples. Mean GRX1-to-actin and TRX1-to-actin signal ratios in β-cells and other tissues were also compared using two-tailed unpaired Student's *t* tests, taking $P < 0.01$ as threshold for significance.

To confirm the microarray data by quantitative RT-PCR, cDNA was prepared from total RNA using random hexamer primers and moloney murine leukemia virus reverse transcriptase (RevertAid H Minus First Strand cDNA synthesis kit; Fermentas, St. Leon-Rot, Germany), following the manufacturer's protocol. Primers and dual-labeled probes (Table 1) were designed using OligoAnalyzer 3.0 software (available from http://biotools.idtdna.com/analyzer/). β-Actin primers and dual-labeled probe were synthesized by Proligo (Paris, France) and those for GRX1 and TRX1 by Eurogentec (Seraing, Belgium). Real-time PCR was performed on a Rotor-Gene 3000 instrument (Corbett Research, Mortlake, Australia), using ABsolute QPCR Mix (ABgene, Epsom, U.K.), according to the manufacturer's instructions. Cycle threshold values were determined by Rotor-Gene 6.0.16 software. All samples were amplified in duplicate reactions, and every experiment was repeated using cDNA samples from independent tissue/cell preparations. In each run, two no-template controls were used for the transcripts under investigation to test for contamination of reagents. Real-time PCR cycling conditions were the following for GRX1: initial denaturation/polymerase activation step at 95°C for 15 min, followed by 45 cycles of denaturation at 95°C for 20 s and annealing/elongation at 57°C for 60 s; for TRX1: the same, but annealing/elongation step at 60°C. For each transcript, serial dilutions of a control template were used to generate standard curves (cycle threshold versus cDNA concentration). Reaction efficiencies (*E*) were calculated from the slopes of the standard curves, according to the following equation: $E = 10(-1/\text{slope})$. All transcripts were amplified with high efficiencies (*E* ranging from 1.83 to 2.00), and linear regression of all standard curves showed a high linear correlation $r^2 > 0.990$). The relative expression of target mRNA levels were calculated as a ratio relative to the β-actin reference mRNA (25).

Protein expression analysis for GRX and TRX. Tissue samples (lung, kidney, liver, brain, skeletal muscle [m. soleus], and fat [intraperitoneal]) were collected from female Sprague Dawley rats. Islets of Langerhans were isolated from rats by collagenase digestion of pancreas followed by handpicking. Tissues and islets were quickly frozen in liquid nitrogen and stored in −80°C until homogenization. Tissue samples, islets, and INS-1E cells (obtained from Dr. C.B. Wollheim, University of Geneva, Geneva, Switzerland) were homogenized in 50 mmol/l TES buffer, pH 7.4, containing 250 mmol/l sucrose, 1 mmol/l EDTA, 0.1 μmol/l EGTA, and complete protease inhibitor cocktail (Roche, Stockholm, Sweden) on ice using an ULTRA-TURRAX (IKA-WERK; Janke & Kunkel, Staufen, Germany) or by repeated aspiration through a needle (Ø0.4 μm). After homogenization, tissue debris was removed by centrifugation (20,000*g*, 15 min, 4°C), and the supernatants were collected. Protein content of the extract was measured using a kit (DC protein assay;

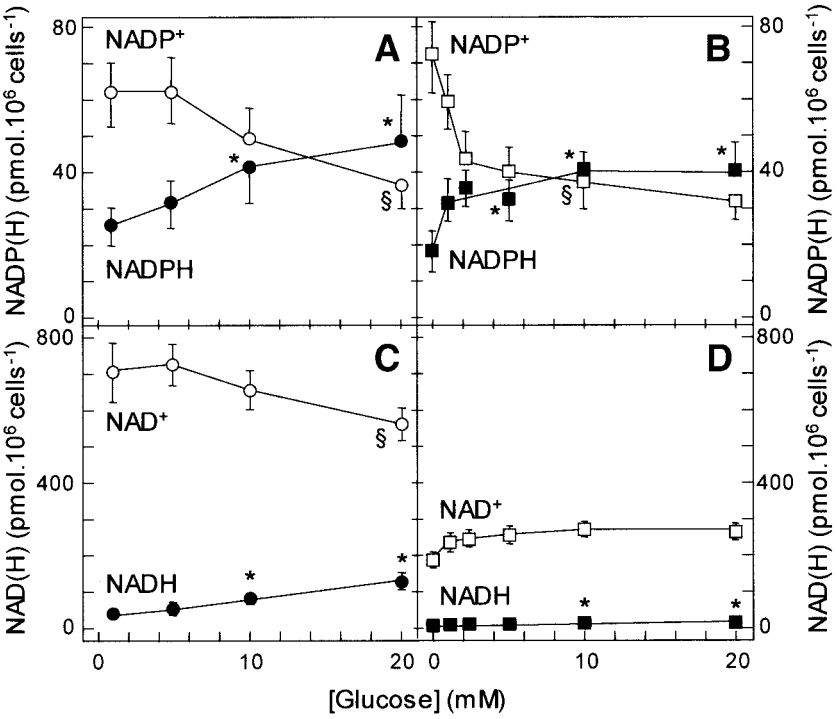

FIG. 1. Glucose effects on the cellular pyridine nucleotide content of rat β-cells and MIN6 cells. The nucleotides were extracted (11,44) after a 30-min incubation with different glucose concentrations as indicated. The effect of glucose is shown upon cellular content of $NADP^+$ and NADPH (*A* and *B*) and NAD^+ and NADH (*C* and *D*) in rat β-cells (*A* and *C*) and MIN6 cells (*B* and *D*). Data are means ± SE of five to nine experiments. Significance of a glucose-induced increase in NAD(*P*)H (P* < 0.05) or decrease in $NAD(P)^+$ (§*P* < 0.05) was calculated versus 1 mmol/l glucose using the unpaired two-tailed Student's *t* test.**

Bio-Rad, Hercules, CA). Forty micrograms of total protein content were electrophoresed on 12% SDS-PAGE, and the separated proteins were transferred onto a polyvinylidine fluoride membrane (Amersham Pharmacia Biotech, Uppsala, Sweden). The membrane was blocked with 5.0% nonfat dry milk in Tris-buffered saline with Tween (pH 7.4; 0.15 mol/l NaCl, 10 mmol/l Tris-HCl, and 0.1% Tween 20) for 1 h at room temperature or overnight at 4°C. After blocking, the membrane was incubated with polyclonal rabbit anti-GRX (1:250) and anti-TRX antibody (1:1,000) (a gift from Dr. Barcena, University of Cordoba, Cordoba, Spain [26]) and monoclonal mouse anti-β actin (1:15,000) in Tris-buffered saline with Tween for 1 h at room temperature. After washing with Tris-buffered saline with Tween, the membrane was incubated with peroxidase-linked anti-rabbit IgG (dilution 1:5,000; Amersham Bioschience) or peroxidase-linked anti-mouse IgG (dilution 1:20,000; Jackson ImmunoResearch,West Groove, PA) for 1 h at room temperature. Detection was done by an enhanced chemiluminescence kit (Amersham). Quantification of protein band densities was calculated by Scion Image software (Scion, Frederick, MD).

Light microscopic GRX and TRX immunostaining. Dispersed islet cells were attached to poly-D-lysine–coated glass coverslips, fixed in 4% paraformaldehyde (Merck, Darmstadt, Germany) for 1 h at 4°C, postfixed in methanol (Merck) for 30 s, and treated with 50 mmol/l ammoniumchloride (Merck) to block free aldehyde groups. Immunofluorescent double staining was performed for insulin with TRX or GRX, respectively, using a guinea pig anti-insulin antibody (a gift of Dr. Van Schravendijk, Diabetes Research Center, Brussels, Belgium) diluted 1:500, and the TRX/GRX antibodies were diluted 1:10 for 60 min at room temperature. Binding was detected with Cy3-labeled anti-rabbit Ig and fluorescein isothiocyanate–labeled anti-guinea pig Ig secondary antibodies (Jackson Immunoresearch Laboratories). Immunofluorescent double staining for SNAP25-TRX and SNAP25-GRX was performed using 1:100 diluted anti–SNAP-25 (Synaptic Systems, Göttingen, Germany) for 60 min at room temperature on membrane patches of dispersed islet cells (27). Controls included the omission of the primary antibody. Preparations were counterstained with 4′,6-diamidino-2-phenylindole, and digital images images were obtained with a Zeiss Axioplan II microscope equipped with a Sensys cooled CCD camera and Quips imaging software (Vysis, Downers Grove, IL).

Electron microscopy and analysis of electron micrographs. Intact pancreatic islets were fixed in 4% paraformaldehyde (Merck, Stockholm, Sweden) with 0.5% glutaraldehyde for 1 h and were then imbedded in Lowicryl and cut into ultrathin sections (60–80 nm) using an LKB MK III Ultratome. GRX immunoreactivity was visualized using a CM 10 electron microscope (Philips, Eindhoven, the Netherlands) after incubation with a rabbit-raised primary antibody (1:60) followed by incubation with a donkey anti-rabbit secondary antibody conjugated with 12-nm gold particles. The subcellular gold particle density was analyzed using the software package from Scion.

RESULTS

The biochemical analysis consisted of cellular extractions and determination of pyridine nucleotide levels after 30-min incubations at different glucose concentrations, using a sensitive enzymatic cycling method. Overall rates of glucose oxidation accelerated about fourfold in both fluorescence-activated cell sorter–purified rat β-cells and in the glucose-responsive murine β-cell line MIN6 when the extracellular substrate level was raised from 1 to 10 mmol/l (data not shown). In both primary β-cells and MIN6 cells, glucose consistently increased the cellular NADPH content (Fig. 1*A*). Assuming a water space of ~0.6 pl per rat β-cell (28) and a uniform nucleotide distribution in the cellular water space, the average NADPH concentration in primary rat β-cells was noted to increase from 42 μmol/l in 1 mmol/l glucose to ~69 μmol/l at 10 mmol/l glucose, which is close to previous biochemical measurements of the NAPDH content in rat islets (13). The steepest increase occurred between the physiological interval of 5–10 mmol/l glucose (Fig. 1*A*), while a further rise up to 80 μmol/l was observed in the presence of 20 mmol/l glucose. The sum of NADPH and $NADP^+$ was unchanged when glucose levels were increased, indicating that a shift of redox state from $NADP^+$ to NADPH occurs, as was expected (Fig. 1*A*). Elevation of glucose caused a significant increase in NADPH and a decrease in $NADP^+$ in both primary β-cells (Fig. 1*A*) and INS1 cells (Fig. 1*B*). Consequently, the glucose-induced rise in the NADPH-to-$NADP^+$ ratio (Fig. 2*A*) was more prominent (almost fourfold over the whole concentration range tested) than that of NADPH content (twofold increase between 1 and 20 mmol/l glucose). In rat β-cells, the ratios averaged 0.40 ± 0.05 vs. 0.93 ± 0.20 at 1 and 10 mmol/l glucose, respectively (n = 5, P = 0.03). Insulin release was measured during static incubations from the same cell types during the same time period as the analysis of pyridine nucleotide content (Fig.

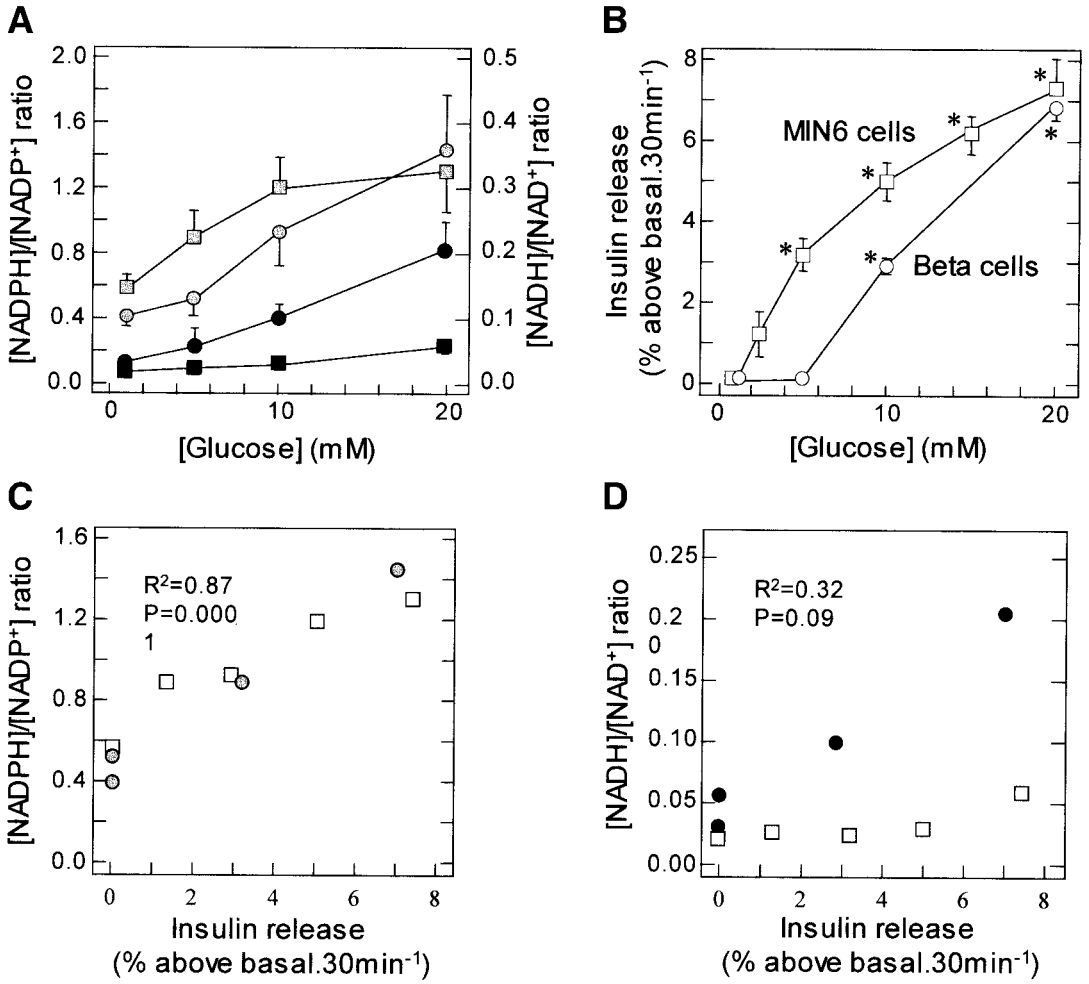

FIG. 2. Glucose-induced insulin release is strongly correlated to the cellular NADPH-to-NADP$^+$ ratio. *A*: Ratios of NADPH to NADP$^+$ (gray symbols) and of NADH to NAD$^+$ (black symbols) in function of extracellular glucose after 30-min incubation of rat primary β-cells (circles) or MIN6 cells (squares). Data are from the same experiments as in Fig. 1. *B*: Insulin release (expressed as percent released of the cellular insulin content above basal per 30 min) from rat β-cells (○) and MIN-6 cells (□). Data are means ± SE of six experiments. Basal release (measured at 1 mmol/l glucose) was 0.6 ± 0.1 and 6.8 ± 1.5% of cellular content in rat β-cells and MIN6 cells, respectively. Insulin content was 28 ± 3 and 1.3 ± 0.1 pg/cell for rat β-cells and MIN6 cells, respectively. Significance of differences in release at a particular glucose concentration versus 1 mmol/l glucose was calculated with the unpaired two-tailed Student's *t* test (*$P < 0.05$). *C*: Correlation between glucose-induced insulin release and cellular NADPH-to-NADP$^+$ ratios in β-cells (◍) and MIN6 cells (□). *D*: Lack of correlation between insulin release and cellular NADH/NAD$^+$ in β-cells (●) and MIN6 cells (□). Data are from the same experiments as shown in Figs. 1 and 2*B*.

2*B*). The cellular NADPH-to-NADP$^+$ ratio correlated strongly to the measured rates of insulin release (R^2 = 0.87, P = 0.0001; Fig. 2*C*). Interestingly, the dose-response curves of the glucose-dependent rise in the NADPH-to-NADP$^+$ ratio and insulin release were hyperbolic in MIN6 cells and sigmoidal in rat β-cells (Fig. 2*A* and *B*).

To assess if changes in the cytosolic NADPH concentration directly influence exocytosis, we next used the standard whole-cell configuration of the patch-clamp technique combined with capacitance measurements of exocytosis (23). As illustrated in Fig. 3, addition of 100 μmol/l NADPH stimulated the increase in membrane capacitance elicited by trains of ten voltage-clamp depolarizations by 84 and 102% over that observed using the control patch electrode solution in both mouse and rat β-cells, respectively. The dose and time dependency of this effect is compatible with a rapid and physiological effect on insulin release for the following reasons. First, significant acceleration of exocytosis was detected well within 1 min of injection of the pyridine nucleotide, indicating a prompt effect on the insulin release machinery (24). Second, the concentration-response curve (Fig. 3*G* and *H*) indicates that 100 μmol/l NADPH is a saturating concentration, and half-maximal activation is attained at 45 μmol/l (i.e., close to the mean concentration estimated in intact β-cells during incubations with physiological glucose concentrations). In the absence of ATP, Ca^{2+}-elicited exocytosis was suppressed and NADPH failed to stimulate release rates (Fig. 4*A* and *B*). Our interpretation of this data is that the action of the pyridine nucleotide is distinct from, and requires, ATP-dependent priming of the dense core granules (23,24). Since glucose not only increases NADPH but also decreases NADP$^+$ (Fig. 1*A*), thereby changing the NADPH-to-NADP$^+$ ratio to a greater extent than that of the absolute NADPH concentration, we next tested if coinjection of NADP$^+$ could also affect exocytosis. Figure 4*C* and *D* shows that the effect of the saturating concentration of NADPH (100 μmol/l) was completely abolished by a threefold molar excess of NADP$^+$, while injection of the oxidized nucleotide alone did not influence exocytosis. Since the NADPH-to-NADP$^+$ ratio shifts in intact rat and mouse β-cells from ~0.4 in the absence of glucose to 1.5 in

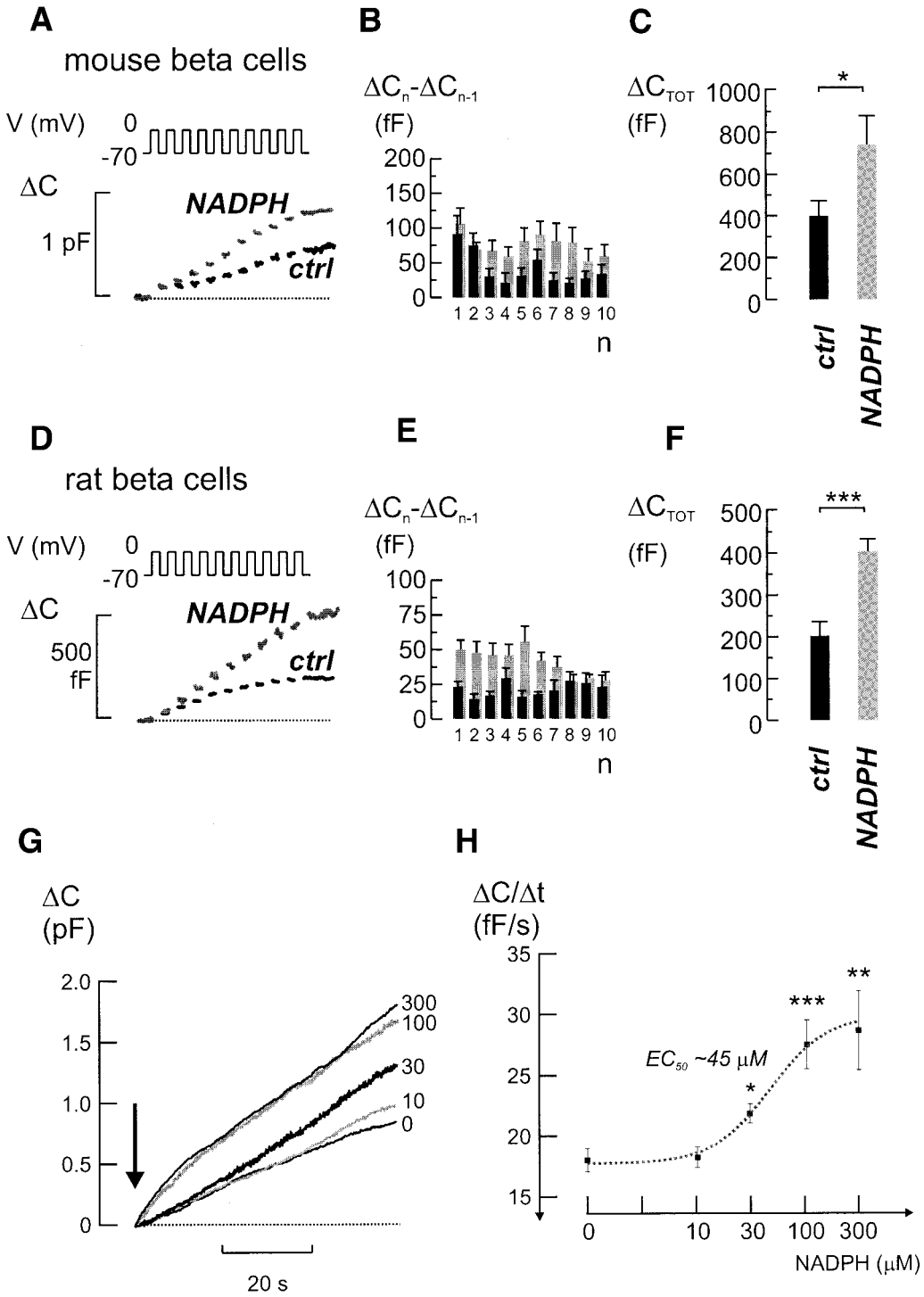

FIG. 3. Dose-dependent potentiation of Ca^{2+}-dependent exocytosis in rodent β-cells. *A*: Exocytosis monitored in mouse β-cells as increases in cell capacitance (ΔC) using the standard whole-cell configuration of the patch-clamp technique and elicited by trains of ten voltage-clamp depolarizations (V) from −70 mV to 0. Experiments were performed using an ATP-containing patch electrode (intracellular) solution, without (in black, *ctrl*) or with NADPH (100 μmol/l; in gray, *NADPH*). *B*: Exocytosis evoked by the individual pulses (ΔC_n-ΔC_{n-1}) in the train stimulation in the absence (■) and in the presence (▨) of NADPH. *C*: Total exocytosis evoked by the train stimulus (ΔC_{TOT}) under control conditions (■) and in the presence (▨) of NADPH. Data are expressed as means ± SE and represent 10 and 5 experiments in the absence and presence of NADPH, respectively. *D–F*: Experimental conditions as in (*A–C*), only performed in rat β-cells. Data in *B* and *C* represent 11 and 18 experiments in the absence and presence of NADPH, respectively. *G*: ΔC evoked by intracellular infusion of a Ca^{2+}- (free $[Ca^{2+}]_I$ ~1.5 μmol/l) and ATP-containing intracellular solution. NADPH was added at a concentration of 10, 30, 100, or 300 μmol/l, as indicated. ↓, indicates the establishment of the standard whole-cell configuration. *H*: Dose-response curve for the stimulatory action of NADPH on β-cell exocytotic rates during the 1st min of recording (ΔC/Δt). The dotted line represents the least-squares fit of the data points to the equation $y = A1+(A2-A1)/1 + 10^{(\log x0-x)p}$, where *y* represents the observed ΔC/Δt, *x* represents the NADPH concentration, *p* represents the Hill coefficient, and A1 and A2 represent ΔC/Δt under nonstimulated and maximally stimulated conditions, respectively. The EC_{50} value was estimated to ~45 μmol/l. Data represent 21, 7, 7, 10, and 13 experiments at NADPH concentrations 0, 10, 30, 100, and 300 μmol/l, respectively. Statistical significances were evaluated using ANOVA followed by Dunnet's post hoc test (P* < 0.05, ***P* < 0.01, ****P* < 0.001).**

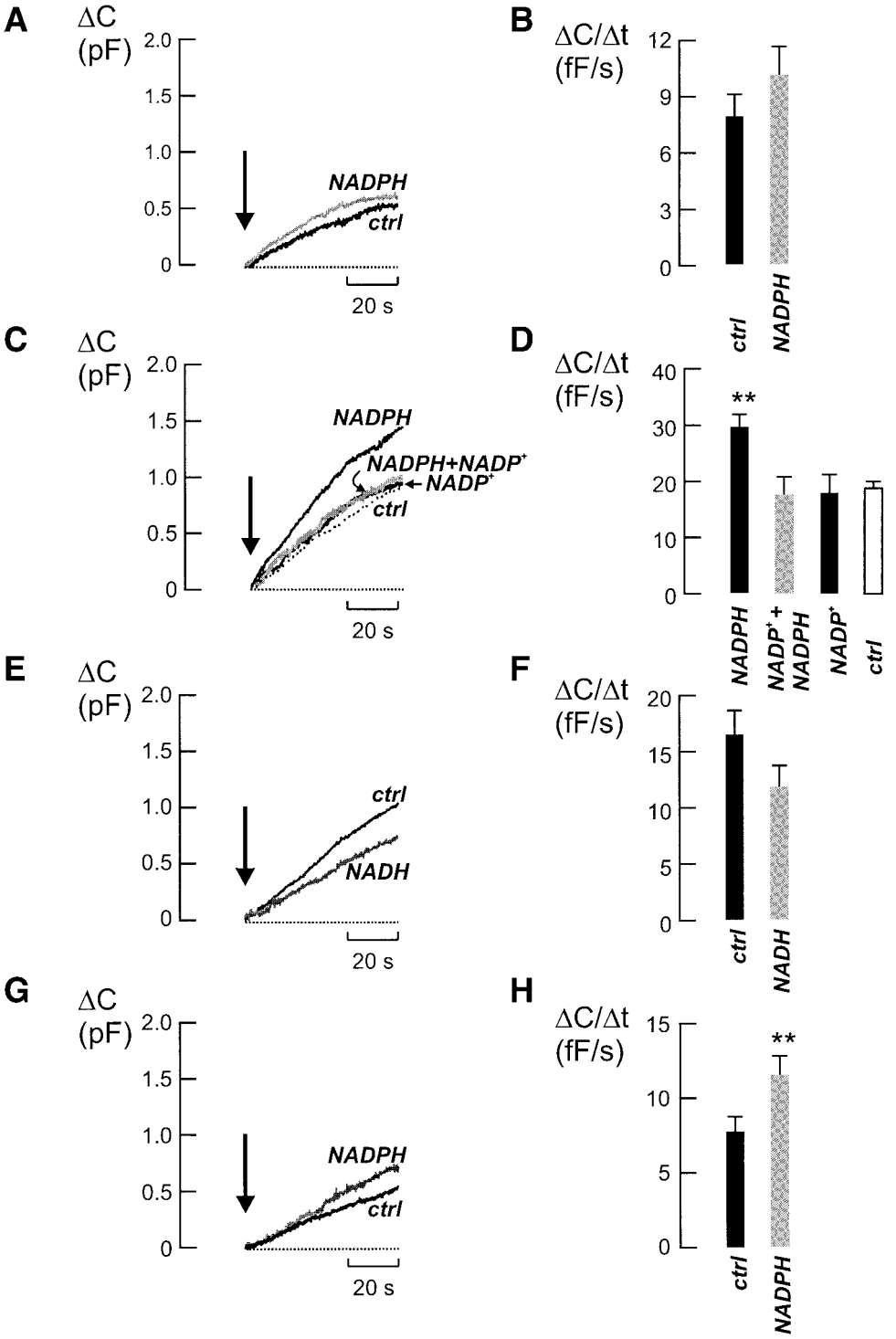

FIG. 4. Properties of NADPH-mediated potentiation of exocytosis. *A*: Failure of NADPH (300 μmol/l; *in gray*) to accelerate increases in ΔC over control (*in black*) in the absence of ATP. Mouse β-cell exocytosis was elicited as in Fig. 3*G* and *H*, except that ATP was omitted from the electrode solution. *B*: Average β-cell exocytotic rates (ΔC/Δt) ± SE, in the absence (■) and in the presence (▨) of NADPH. Data are from eight experiments made with and without NADPH, in the absence of ATP. *C*: ΔC elicited using the Ca^{2+}- and ATP-containing pipette solution (cf. Fig. 3*G* and *H*). In the simultaneous excess presence of its oxidized $NADP^+$ form (300 μmol/l), NADPH (100 μmol/l; *in gray*) fails to stimulate single-cell insulin release over that observed under control conditions (*dotted*). It was ascertained that 300 μmol/l $NADP^+$ itself did not affect exocytosis (*in black*). *D*: Mean ΔC/Δt ± SE in the presence of NADPH only (■), in the simultaneous presence of NADPH and $NADP^+$ (▨), with $NADP^+$ alone added (■), and when using the control pipette solution (□). Data are from 8 to 24 experiments under the respective conditions. *E* and *F*: Experimental conditions as in (*C* and *D*), but NADH (300 μmol/l) was added instead of NADPH. Data represent six and eight experiments in the absence and presence of NADH, respectively. *G*: Stimulatory action of NADPH (300 μmol/l; *in gray*) on ΔC elicited in catecholamine-releasing PC12 cells compared with infusing the control pipette solution (*in black*). *H*: Average ΔC/Δt ± SE denoting 9 and 10 PC12 cell experiments with and without NADPH, respectively. Statistical significance was calculated as in Fig. 3 ($P < 0.01$).**

the presence of 20 mmol/l glucose (Fig. 2*A*), $NADP^+$ appears to be an antagonist of the effect of NADPH so that glucose has two actions on the putative pyridine nucleotide–sensitive target(s): *1*) generation of an activator and *2*) removal of an inactivator. This situation would be analogous to the glucose-induced shift in the adenine nucleotides ADP and ATP (29), which have inverse effects on K_{ATP} channels (30).

To further clarify the roles of pyridine nucleotides as putative signaling molecules for exocytosis, glucose-induced changes in NADH were measured and effects of NADH on exocytosis were quantified. While glucose raised the content of NADH in rat β-cells (Fig. 1*C*) and MIN6 cells (Fig. 1*D*), this effect was small over the tested range of glucose concentrations. Furthermore, there was no detectable decrease in NAD^+ in MIN6 cells, and the measured NADH-to-NAD^+ ratios in these cells were between 3 and 10 times lower than in rat β-cells, the latter being close to that previously reported in rat islets ex vivo (13). Consequently, in the pooled dataset of β-cells and MIN6 cells, the cellular NADH-to-NAD^+ ratio was not correlated to the rate of insulin release (Fig. 2*D*), but a positive correlation

might be present when data of primary β-cells are considered separately from those of MIN6 cells. Moreover, the glucose depencency of the NADH-to-NAD^+ ratio was linear rather than hyperbolic or sigmoidal (Fig. 2*A*). At the electrophysiological level, the addition of 300 μmol/l NADH in the patch-clamp analysis did not mimic the effects of NADPH. As can been seen in Fig. 4*E* and *F*, this condition did not stimulate exocytosis; in fact, a modest but consistent inhibition was observed. As such, these data not only exclude a nonspecific reaction but makes it also unlikely that the effects on insulin exocytosis are causally related to the glycolytic production of NADH (18,19). To address the issue of cellular specificity, our experimental design was repeated in catecholamine-releasing PC12 cells, a well-characterized model of regulated exocytosis (Fig. 4*G* and *H*). Similarly, in this model, the intracellular addition of NADPH elevated Ca^{2+}-elicited membrane capacitance by 50%, suggesting that this pyridine nucleotide plays a novel and thus far unrecognized role in the potentiation of Ca^{2+}-regulated exocytosis.

To explore the mechanism of the NADPH-mediated actions on the exocytotic machinery, we assessed the possibility that particular redox acceptor proteins (20) might mediate the effect of NADPH on exocytosis. In line with this hypothesis, we examined the expression level of the GRX1 and TRX1 genes at both the mRNA (Fig. 5*A*) and protein (Fig. 5*B*) levels. Using Affymetrix microarrays, we observed that expression signals of GRX1 mRNA were significantly higher in pancreatic β-cells than in flow-sorted islet non–β-cells as well as seven tested extrapancreatic tissues (Fig. 5*A*; $P < 0.01$ for all comparisons). Moreover, all 72 pairwise comparisons of the 3 β-cell samples, with 24 samples from other cells and tissue (Affymetrix GCOS program), gave "increased in β-cells" calls, the mean signal log ratio of these comparisons being 1.7 and the lowest value 0.9. On the contrary, TRX1 mRNA signals in β-cells were significantly lower than those in liver, fat, lung, and kidney ($P < 0.001$); Fig. 5*B*). These data were corroborated by quantitative RT-PCR analaysis, with a few minor differences like a higher GRX1 mRNA signal in liver and a lower TRX1 signal in adipose tissue. At the protein level, we observed high expression of GRX in both pancreatic islets and in INS1 cells as well as in brain (Fig. 5*B*) and intermediate signals in adipose tissue. Interestingly, the TRX1 protein level was highest in islets and INS1 cells and lowest in liver and muscle, while the inverse situation was observed for mRNA levels.

To assess whether islet TRX and GRX can be localized in β-cells, we performed light microscopic analysis of dissociated islet rat cells. Figure 6*A* shows that TRX and GRX immunostaining of β-cells using polyclonal TRX and GRX antibodies (26) exhibits a punctuate distribution pattern. Higher-resolution immunostaining of the inner face of the plasma membrane suggests the two redox proteins are present in a nonuniform clustered distribution that is disctinct from SNAP25 in lipid rafts (Fig. 6*B*). At the electron microscopic level, it was further documented that GRX preferentially localizes in particular subcellular domains such as the nucleus and secretory granules (Fig. 6*C* and *D*).

To assess the potential functional relevance of GRX and TRX for insulin secretion, we next studied the effect of an altered GRX-to-TRX ratio upon NADPH-induced exocytosis by coadministration of GRX or TRX together with NADPH (100 μmol/l) in the intracellular pipette solution. As is shown in Fig. 7*A* and *B*, a supplement of GRX (1 μmol/l) further augmented NADPH- and depolarization-elicited exocytosis by 54% ($P < 0.05$); on the contrary, addition of extra TRX (1 μmol/l) completely counteracted the stimulatory action of NADPH and reduced the exocytotic response by 66% ($P < 0.01$). It was verified that the stimulation of insulin release by GRX was specific for NADPH. Indeed, when NADH (100 μmol/l) was included in the intracellular solution instead of NADPH, GRX failed to enhance depolarization-evoked exocytosis (172 ± 28 fF, $n = 6$ and 210 ± 44, $n = 13$, with and without GRX, respectively, means ± SE). Moreover, in the presence of a permissive NADPH concentration (100 μmol/l) but in the presence of a threefold molar excess of $NADP^+$, GRX failed to enhance depolarization-evoked exocytosis (average capacitance increase 405 ± 35 and 408 ± 32 fF without and with GRX, respectively, $n = 5$).

The activity of GRX is under the control of the glutathione system (31) to mediate several important NADPH-dependent cellular processes, such as DNA synthesis (32), protein folding and transcriptional regulation (33), signal transduction (31), as well as defense against oxidative stress and apoptosis (34,35). Therefore, it can be anticipated that the reduced form of glutathione, acting as an intermediate between NADPH and reduced GRX, would also potentiate Ca^{2+}-dependent exocytosis. As is shown in Fig. 7*C* and *D*, intracellular addition of glutathione (1 mmol/l) stimulated exocytosis by 46% ($P < 0.05$).

DISCUSSION

The present report has studied redox regulation of insulin release following the hypothesis that the reducing power of the cells, in combination with the expression of the redox proteins GRX1 and TRX1, is critical for the amplification of the glucose-induced Ca^{2+}-mediated signaling pathway. Our biochemical analysis of the four pyridine nucleotides confirms earlier studies (12,13) showing that both NADPH/$NADP^+$ and NADH/NAP^+ acutely increase in β-cells when glucose in the extracellular medium rises. To our knowledge, however, this study is the first to demonstrate via electrophysiological recordings that an experimentally imposed rise in the NADPH-to-$NADP^+$ ratio in itself does cause exocytosis, amplifying the Ca^{2+}- and ATP-mediated response. The specificity of this phenomenon is underlined by showing that *1*) alterations in the NADH-to-NAD^+ ratio do not have such an effect and *2*) that the effectiveness of the NADPH-to-$NADP^+$ ratio upon exocytosis can be further modulated by GRX1 and TRX1, the two best-known acceptor proteins for NADPH electrons (20).

GRX1 has previously been proposed to play a role in exocytosis on basis of its immunohistochemical localization in synaptic terminals in the neurohypophysis (26), and an increased NADPH-to-$NADP^+$ ratio has been linked to the intense wave of exocytosis of cortical granules oocyte fertilization (36). Redox-regulated posttranslational modification of exocytosis-regulating t-SNARE proteins has been proposed to result in an increased rate of maturation, or priming, of secretory vesicles in yeast (37). A similar

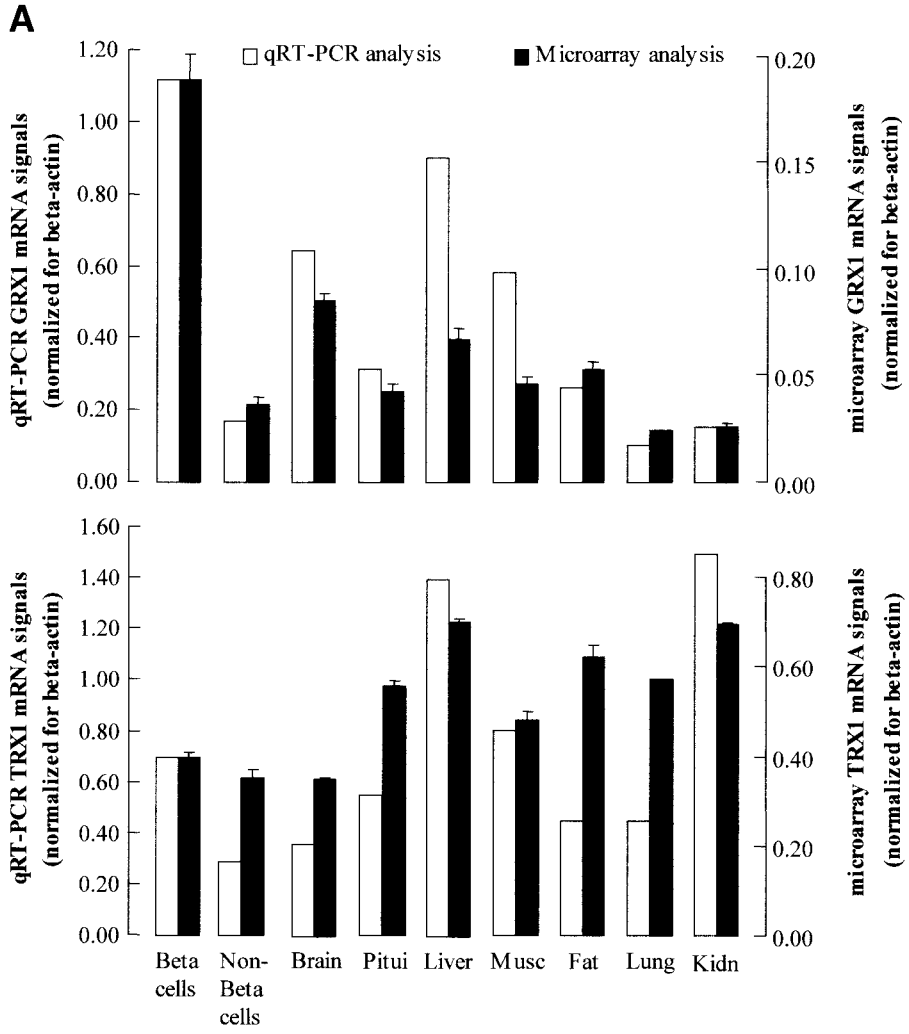

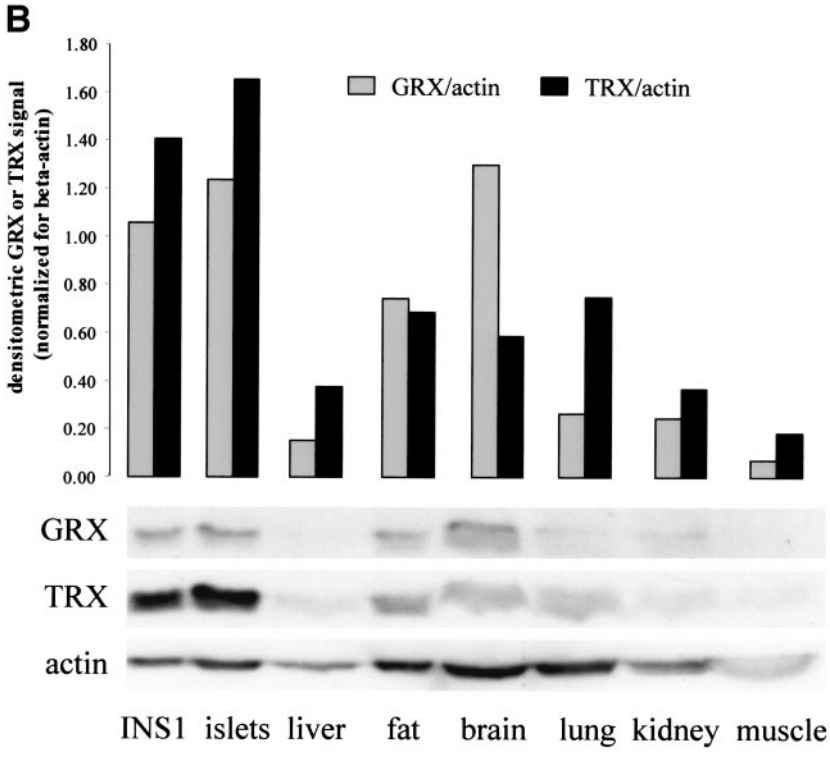

FIG. 5. TRX1 and GRX1 mRNA and protein expression in β-cells. *A*: mRNA expression analysis was performed by Affymetrix rat 230A microarrays (means ± SE of three experiments) and via real-time RT-PCR (means of two experiments). RNA was extracted and analyzed as described in experimental procedures. Statistical analysis of the array data indicates that the mean GRX1-to-actin ratio in β-cells is significantly higher than that in each of the compared cells/tissues ($P < 0.01$). TRX1 mRNA expression in β-cells was lower in β-cells than in liver and muscle ($P < 0.001$ for the microarray measurements). *B*: Immunoblots of total protein extracted from INS1 cells, rat islets and rat liver, adipose tissue, brain, lung, kidney, and skeletal muscle, using polyclonal antisera against GRX and TRX (26). Data in the graph correspond to mean GRX and TRX signals normalized for β-actin from two independent experiments. The blots of one such experiment are shown in the bottom panel. Please note that liver and muscle have the lowest TRX protein expression and islets the highest.

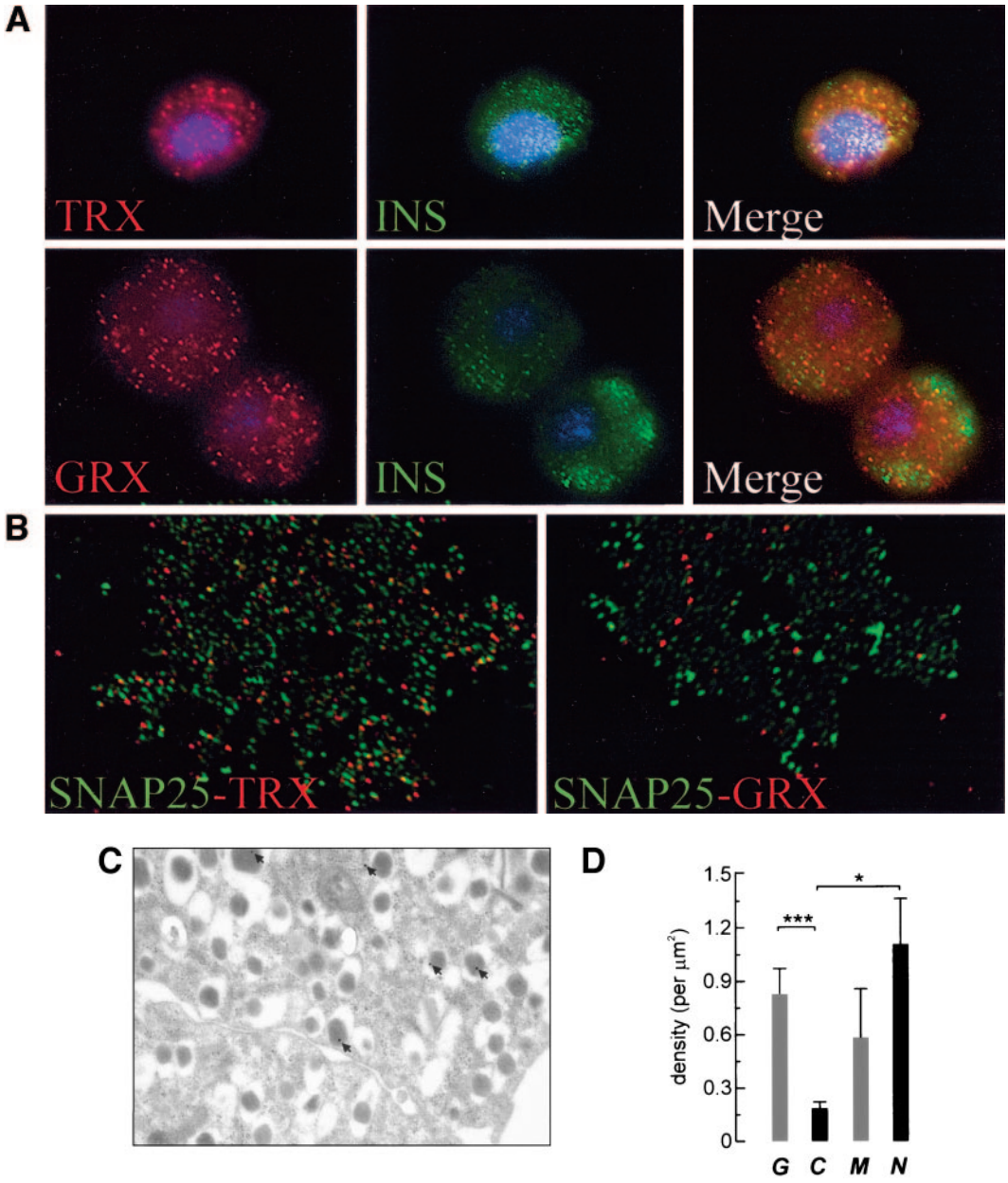

FIG. 6. Immunostaining of GRX and TRX in rat β-cells. *A*: Colocalization of TRX/insulin and GRX/insulin in rat dissociated islet cells. *B*: Heterogenous localization of GRX and TRX at the inner side of plasma membrane that is distinct from SNAP25. Punctuate immunostaining of TRX (*left*) and GRX (*right*) is in distinct membrane domains from SNAP-25 staining (green). *C*: Electron micrograph of a pancreatic β-cell with GRX localization visualized by immunogold labeling (arrows, *left*). Average gold particle density (per μm²) in nucleus (*N*), cytosol (*C*), mitochondria (*M*), and insulin granules (*G*), as indicated. Data represent averages ± SE in 15 micrographs. Statistical significance was calculated as in Fig. 3 (*$P < 0.05$, ***$P < 0.001$).

accelerated formation of mature insulin granules by NADPH/GRX may provide an explanation for the potentiating affect of NADPH on exocytosis evoked by Ca^{2+} and ATP in neuroendocrine cells, and we propose in this report that regulated exocytosis is linked to cellular metabolism via the cellular redox state. The sequence of events seems to be nutrient-induced reduction of $NADP^+$ and flow of electrons from NADPH to glutathione, GRX1, and TRX1. This pathway would be particularly important for the pancreatic β-cell, which has to match the extracellular glucose concentration to the rate of insulin release. Indeed, this idea is consistent with previous reports that cataplerosis of citrate (15) as well as pyruvate cycling (17) in β-cells is linked to insulin secretion. Furthermore, β-cells with a high insulin secretory competence upregulate mRNA expression encoding NADPH-generating pathways such as glucose-6-phosphate dehydrogenase (16) and ATP-citrate lyase (16).

Our results (mRNA/protein expression studies and electrophysiological analysis of exocytosis) suggest that both the expression level of GRX/TRX in the β-cell as well as the NADPH/$NADP^+$ redox status are important factors for the regulation of exocytosis. It is conceivable that such redox regulatory system is further regulated by accessory proteins such as the thioredoxin regulatory protein (VDUP1), whose expression is glucose dependent (38,39). Our data are of particular interest in the context of human type 2 diabetes, in which there is dysregulation of insulin

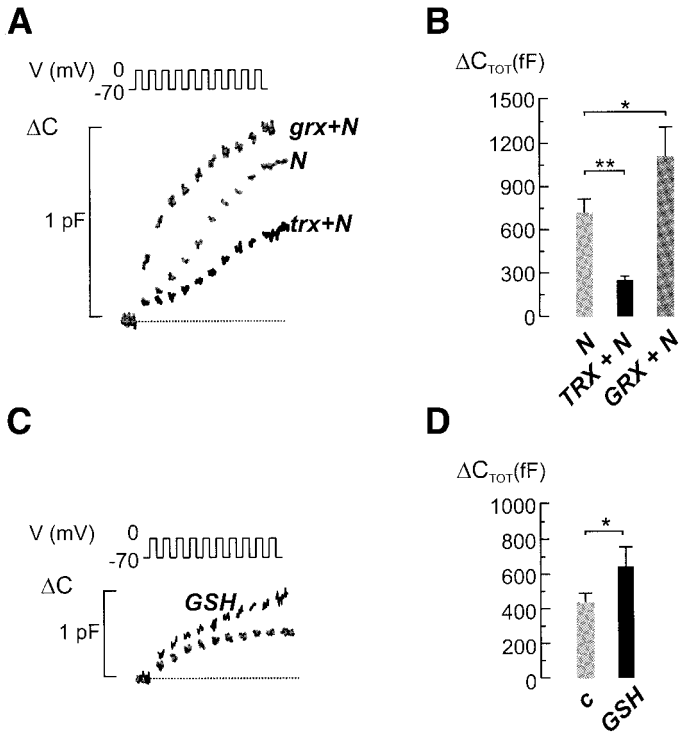

FIG. 7. Mechanism of NADPH action on the exocytotic machinery. *A*: Depolarisation-evoked ΔC in mouse β-cells in the intracellular presence of NADPH (100 μmol/l; *N*, *in gray*), with GRX (1 μmol/l) added to the NADPH-containing intracellular solution (grx+*N*, *in gray*), in the presence of TRX (1 μmol/l; trx+N, *in black*) *B*: Total exocytosis evoked by the train stimulus (ΔC$_{TOT}$) in the presence of NADPH (N, ▨), TRX and NADPH (trx+N, ■), and GRX and NADPH (grx+N, ▨). Data are expressed as means ± SE and represent 10, 5, and 7 experiments in the presence of NADPH only, TRX and NADPH, and GRX and NADPH, respectively. *C* and *D*: As in (*A* and *B*), but the experiments were performed using a pipette solution without NADPH but instead the reduced form of glutathione (GSH; 1 mmol/l, *in black*) was added to the control intracellular solution (*in gray*). Data are from six experiments, in the presence (■) as well as in the absence (▨) of reduced glutathione, respectively.

release by glucose. In addition to initiating electrical activity by ATP-dependent closure of the β-cell K_{ATP} channels, glucose metabolism also exerts a potentiating action on the insulin release apparatus via a K_{ATP} channel–independent pathway (5). The latter pathway is impaired in animal models of type 2 diabetes (40) and appears to be defective in human type 2 diabetic patients (41). The identity of the alternative metabolic signal that amplifies insulin secretion has remained an unsettled issue, particularly with respect to the question of whether glutamate (formed from the citric acid cycle intermediate α-ketoglutarate) fulfills this function (42,43). Without being mutually exclusive to the glutamate hypothesis (42), our data suggest that the glucose-mediated generation of NADPH and the reduction of GRX and TRX are newly identified components of redox regulation of exocytosis.

ACKNOWLEDGMENTS

This work was supported by grants from the Swedish Research Council (no. 12234), the European Foundation for the Study of Diabetes, and the Novo Nordisk and Crafoord Foundations to E.R. and from the Fonds voor Wetenschappelijk Onderzoek-Vlaanderen (FWO-Vlaanderen) (G.0130.99), the Juvenile Diabetes Research Foundation (1-2002-801), and the Katholieke Universiteit-Leuven (GOA/2004/11) to F.S. The position of R.I. was partly funded by Lund University, and those of S.D. (research assistant) and F.S. (research professor) were supported by the FWO-Vlaanderen. MIN6 cells were kindly donated by H. Ishihara and Y. Oka (Tohoku University Graduate School of Medicine, Sendai, Japan). INS-1E cells were a gift from Dr. C.B. Wollheim (University of Geneva, Geneva, Switzerland). Affinity-purified polyclonal rabbit anti-rat GRX and TRX antisera were kindly provided by Dr. J.A. Barcena (Department of Biochemistry and Molecular Biology, University of Cordoba, Cordoba, Spain; see [26]).

All experiments were approved by the ethical committees at Lund University, Lund, Sweden; the Katholieke Universiteit, Leuven, Belgium; and the Vrije Universiteit, Brussels, Belgium. We thank G. Stangé for rat β-cell purifications, V. Berger and G. Schoonjans for help with the insulin assays, L. Van Lommel for help with the microarray RNA analysis, L. Eliasson for help with the electron microscopy, S. Hinke for manuscript review, and H. Mulder for valuable discussions.

REFERENCES

1. Newgard CB, McGarry JD: Metabolic coupling factors in pancreatic beta-cell signal transduction. *Annu Rev Biochem* 64:689–719, 1995
2. Corkey BE, Deeney JT, Yaney GC, Tornheim K, Prentki M: The role of long-chain fatty acyl-CoA esters in beta-cell signal transduction. *J Nutr* 130 (Suppl. 2S):299S–304S, 2000
3. Schuit FC, Huypens P, Heimberg H, Pipeleers DG: Glucose sensing in pancreatic β-cells: a model for the study of other glucose-regulated cells in gut, pancreas, and hypothalamus. *Diabetes* 50:1–11, 2001
4. Ashcroft FM, Harrison DE, Ashcroft SJ: Glucose induces closure of single potassium channels in isolated rat pancreatic beta-cells. *Nature* 312:446–448, 1984
5. Henquin JC: Triggering and amplifying pathways of regulation of insulin secretion by glucose. *Diabetes* 49:1751–1760, 2000
6. Ammon HP, Abdel-hamid M: Potentiation of the insulin-releasing capacity of tolbutamide by thiols: studies on the isolated perfused pancreas. *Naunyn Schmiedebergs Arch Pharmacol* 317:262–267, 1981
7. Van De Winkel M, Pipeleers D: Autofluorescence-activated cell sorting of pancreatic islet cells: purification of insulin-containing B-cells according to glucose-induced changes in cellular redox state. *Biochem Biophys Res Commun* 114:835–842, 1983
8. Kiekens R, In't Veld P, Mahler T, Schuit F, Van De WM, Pipeleers D: Differences in glucose recognition by individual rat pancreatic B cells are associated with intercellular differences in glucose-induced biosynthetic activity. *J Clin Invest* 89:117–125, 1992
9. Pralong WF, Bartley C, Wollheim CB: Single islet beta-cell stimulation by nutrients: relationship between pyridine nucleotides, cytosolic Ca2+ and secretion. *EMBO J* 9:53–60, 1990
10. Bennett BD, Jetton TL, Ying G, Magnuson MA, Piston DW: Quantitative subcellular imaging of glucose metabolism within intact pancreatic islets. *J Biol Chem* 271:3647–3651, 1996
11. Malaisse WJ, Hutton JC, Kawazu S, Sener A: The stimulus-secretion coupling of glucose-induced insulin release: metabolic effects of menadione in isolated islets. *Eur J Biochem* 87:121–130, 1978
12. Trus MD, Hintz CS, Weinstein JB, Williams AD, Pagliara AS, Matschinsky FM: A comparison of the effects of glucose and acetylcholine on insulin release and intermediary metabolism in rat pancreatic islets. *J Biol Chem* 254:3921–3929, 1979
13. Trus M, Warner H, Matschinsky F: Effects of glucose on insulin release and on intermediary metabolism of isolated perifused pancreatic islets from fed and fasted rats. *Diabetes* 29:1–14, 1980
14. Heimberg H, De Vos A, Vandercammen A, Van Schaftingen E, Pipeleers D, Schuit F: Heterogeneity in glucose sensitivity among pancreatic beta-cells is correlated to differences in glucose phosphorylation rather than glucose transport. *EMBO J* 12:2873–2879, 1993
15. Farfari S, Schulz V, Corkey B, Prentki M: Glucose-regulated anaplerosis and cataplerosis in pancreatic β-cells: possible implication of a pyruvate/citrate shuttle in insulin secretion. *Diabetes* 49:718–726, 2000
16. Flamez D, Berger V, Kruhoffer M, Orntoft T, Pipeleers D, Schuit FC: Critical

role for cataplerosis via citrate in glucose-regulated insulin release. *Diabetes* 51:2018–2024, 2002
17. Lu D, Mulder H, Zhao P, Burgess SC, Jensen MV, Kamzolova S, Newgard CB, Sherry AD: 13C NMR isotopomer analysis reveals a connection between pyruvate cycling and glucose-stimulated insulin secretion (GSIS). *Proc Natl Acad Sci U S A* 99:2708–2713, 2002
18. Dukes ID, McIntyre MS, Mertz RJ, Philipson LH, Roe MW, Spencer B, Worley JF 3rd: Dependence on NADH produced during glycolysis for beta-cell glucose signaling. *J Biol Chem* 269:10979–10982, 1994
19. Eto K, Tsubamoto Y, Terauchi Y, Sugiyama T, Kishimoto T, Takahashi N, Yamauchi N, Kubota N, Murayama S, Aizawa T, Akanuma Y, Aizawa S, Kasai H, Yazaki Y, Kadowaki T: Role of NADH shuttle system in glucose-induced activation of mitochondrial metabolism and insulin secretion. *Science* 283:981–985, 1999
20. Holmgren A: Antioxidant function of thioredoxin and glutaredoxin systems. *Antioxid Redox Signal* 2:811–820, 2000
21. Pipeleers DG, in't Veld PA, Van De WM, Maes E, Schuit FC, Gepts W: A new in vitro model for the study of pancreatic A and B cells. *Endocrinology* 117:806–816, 1985
22. Ishihara H, Asano T, Tsukuda K, Katagiri H, Inukai K, Anai M, Kikuchi M, Yazaki Y, Miyazaki JI, Oka Y: Pancreatic beta cell line MIN6 exhibits characteristics of glucose metabolism and glucose-stimulated insulin secretion similar to those of normal islets. *Diabetologia* 36:1139–1145, 1993
23. Eliasson L, Ma X, Renstrom E, Barg S, Berggren PO, Galvanovskis J, Gromada J, Jing X, Lundquist I, Salehi A, Sewing S, Rorsman P: SUR1 regulates PKA-independent cAMP-induced granule priming in mouse pancreatic B-cells. *J Gen Physiol* 121:181–197, 2003
24. Renstrom E, Eliasson L, Bokvist K, Rorsman P: Cooling inhibits exocytosis in single mouse pancreatic B-cells by suppression of granule mobilization. *J Physiol* 494 (Pt 1):41–52, 1996
25. Pfaffl MW: A new mathematical model for relative quantification in real-time RT-PCR. *Nucleic Acid Res* 29:e45, 2001
26. Padilla CA, Martinez-Galisteo E, Lopez-Barea J, Holmgren A, Barcena JA: Immunolocalization of thioredoxin and glutaredoxin in mammalian hypophysis. *Mol Cell Endocrinol* 85:1–12, 1992
27. Lang T, Bruns D, Wenzel D, Riedel D, Holroyd P, Thiele C, Jahn R: SNAREs are concentrated in cholesterol-dependent clusters that define docking and fusion sites for exocytosis. *EMBO J* 20:2202–2213, 2001
28. Heimberg H, De Vos A, Pipeleers D, Thorens B, Schuit F: Differences in glucose transporter gene expression between rat pancreatic alpha- and beta-cells are correlated to differences in glucose transport but not in glucose utilization. *J Biol Chem* 270:8971–8975, 1995
29. Detimary P, Dejonghe S, Ling Z, Pipeleers D, Schuit F, Henquin JC: The changes in adenine nucleotides measured in glucose-stimulated rodent islets occur in beta cells but not in alpha cells and are also observed in human islets. *J Biol Chem* 273:33905–33908, 1998
30. Tucker SJ, Ashcroft FM: A touching case of channel regulation: the ATP-sensitive K+ channel. *Curr Opin Neurobiol* 8:316–320, 1998
31. Fernandes AP, Holmgren A: Glutaredoxins: glutathione-dependent redox enzymes with functions far beyond a simple thioredoxin backup system. *Antioxid Redox Signal* 6:63–74, 2004
32. Holmgren A: Hydrogen donor system for Escherichia coli ribonucleoside-diphosphate reductase dependent upon glutathione. *Proc Natl Acad Sci U S A* 73:2275–2279, 1976
33. Lundstrom-Ljung J, Holmgren A: Glutaredoxin accelerates glutathione-dependent folding of reduced ribonuclease A together with protein disulfide-isomerase. *J Biol Chem* 270:7822–7828, 1995
34. Daily D, Vlamis-Gardikas A, Offen D, Mittelman L, Melamed E, Holmgren A, Barzilai A: Glutaredoxin protects cerebellar granule neurons from dopamine-induced apoptosis by activating NF-kappa B via Ref-1. *J Biol Chem* 276:1335–1344, 2001
35. Song JJ, Lee YJ: Differential role of glutaredoxin and thioredoxin in metabolic oxidative stress-induced activation of apoptosis signal-regulating kinase 1. *Biochem J* 373:845–853, 2003
36. Eisen A, Kiehart DP, Wieland SJ, Reynolds GT: Temporal sequence and spatial distribution of early events of fertilization in single sea urchin eggs. *J Cell Biol* 99:1647–1654, 1984
37. Gerst JE: SNARE regulators: matchmakers and matchbreakers. *Biochim Biophys Acta* 1641:99–110, 2003
38. Shalev A, Pise-Masison CA, Radonovich M, Hoffmann SC, Hirshberg B, Brady JN, Harlan DM: Oligonucleotide microarray analysis of intact human pancreatic islets: identification of glucose-responsive genes and a highly regulated TGFbeta signaling pathway. *Endocrinology* 143:3695–3698, 2002
39. Minn AH, Hafele C, Shalev A: Thioredoxin-interacting protein is stimulated by glucose through a carbohydrate response element and induces {beta}-cell apoptosis. *Endocrinology* 146:2397–2405, 2005
40. Hughes SJ, Faehling M, Thorneley CW, Proks P, Ashcroft FM, Smith PA: Electrophysiological and metabolic characterization of single β-cells and islets from diabetic GK rats. *Diabetes* 47:73–81, 1998
41. Ward WK, Bolgiano DC, McKnight B, Halter JB, Porte D Jr: Diminished B cell secretory capacity in patients with noninsulin-dependent diabetes mellitus. *J Clin Invest* 74:1318–1328, 1984
42. Maechler P, Wollheim CB: Mitochondrial glutamate acts as a messenger in glucose-induced insulin exocytosis. *Nature* 402:685–689, 1999
43. MacDonald MJ, Fahien LA: Glutamate is not a messenger in insulin secretion. *J Biol Chem* 275:34025–34027, 2000
44. Lowry OH: Amplification by enzymatic cycling. *Mol Cell Biochem* 32:135–146, 1980